Title: Dissolved Organic Carbon Sorption Dynamics in Tidal Marsh Soils

Running head: Tidal Marsh Soil Sorption Dynamics

Article Type: Research Article

Authors: Andrew J Pinsonneault[1a], J Patrick Megonigal[1b], Patrick J Neale[1c], Maria Tzortziou[2d], Elizabeth A Canuel[3e], Christina R. Pondell[3f], Hannah Morrissette[4g], Jonathan S. Lefcheck[1f]

[1]Smithsonian Environmental Research Center, Edgewater, Maryland, USA

[2]Department of Earth & Atmospheric Science, City College of New York, New York, New York, USA

[3]Virginia Institute of Marine Science, William & Mary, Gloucester Point, Virginia, USA

[4]University of Maryland Center for Environmental Science, Cambridge, Maryland, USA

[a]Corresponding author contact: PinsonneaultA@si.edu, phone: (+1) 443-482-2441, fax: (+1) 202-312-1934

[b]megonigalp@si.edu

[c]nealep@si.edu

[d]mtzortziou@ccny.cuny.edu

[e]ecanuel@vims.edu

[f]cpondell@vims.edu

[g]hmorrissette@umces.edu

[h]lefcheckj@si.edu

Keywords: Langmuir isotherms, tidal marshes, soils, iron, aluminum

Abstract

Coastal wetlands are significant sources of dissolved organic carbon (DOC) to adjacent waters and, consequently, exert a strong influence on the quantity and quality of DOC exported to the coastal oceans. Our understanding of the factors that control the exchange of DOC at the tidal marsh-estuarine interface, however, remains limited. We hypothesize that tidal marsh soils act as a regulator and that their physical characteristics, such as organic carbon content and mineral phase composition, are key controls on DOC exchange between soil surfaces and both surface and interstitial waters. To test this hypothesis, we generated traditional Langmuir sorption isotherms using anaerobic batch incubations of four tidal wetland soils, representing a range of soil organic carbon content (1.77 ± 0.12 % to 36.2 ± 2.2%) and salinity regimes (freshwater to mixoeuhaline), across four salinity treatments. Results suggest that the maximum soil sorption capacity (Q_{max}) and DOC binding affinity (K) increase and decrease with greater salinity, respectively, though the enhancement of Q_{max} is somewhat mitigated in soils richer in poorly crystalline iron minerals ([PC-Fe]). Initial natively sorbed organic carbon (C_0) showed a significant positive correlation with soil specific surface area and K showed a moderate yet significant positive correlation with [PC-Fe]. Taken together, these results point to a strong mineralogical control on tidal marsh sorption dynamics and a complex physicochemical response of those dynamics to salinity in tidal marsh soils.

Introduction

Tidal wetlands are hotspots of biogeochemical exchange and transformation as well as some of the most productive ecosystems on Earth with net primary productivity commonly exceeding 600 g C m^{-2} y^{-1} in the temperate zone (Mendelssohn and Morris 2000; Megonigal and Neubauer 2009). These ecosystems occur in geomorphic settings that promote the exchange of water, solutes, and particulates with adjacent estuaries (Wang and Cai, 2004; Tzortziou et al., 2011; Megonigal and Neubauer 2009), and they serve as significant sources of dissolved organic carbon (DOC) to the coastal ocean (Childers et al. 2000; Tzortziou et al. 2008; Tobias and Neubauer 2009; Najjar et al. 2018). The export of total organic carbon (TOC), of which DOC is a part, from tidal wetlands to coastal waters of the eastern United States alone is 1.2 – 2.9 Tg-C y^{-1} (Herrmann et al., 2015), supporting vital ecological functions such as microbial respiration, UV adsorption, and nutrient flux (Marschner and Kalbitz, 2003; Moore, 2009). Despite the importance of wetland DOC export to estuarine ecosystem metabolism, there is relatively little understood about the processes that regulate DOC exchange at the tidal-estuarine interface.

Previous tidal marsh studies have reported that both DOC concentration ([DOC]) and optical characteristics differ dramatically between flooding tide and ebbing tide, with the ebb tide exhibiting greater concentration, molecular weight, and aromaticity (Tzortziou et al., 2008). DOC optical characteristics are a sensitive indicator of chemical composition (Hansen et al. 2016) and have been used to monitor variation in DOC sources and sinks over tidal cycles (Clark et al., 2008; Tzortziou et al. 2008). Sources of marsh DOC include leachates from senescent vegetation (Maie et al. 2006), exudates from macrophytes, microalgae, and phytoplankton, and the soil organic matter that forms during the advanced stages of decomposition of these sources. Complex interactions between biological and physical processes regulate the contribution of

carbon sources to the DOC in interstitial waters that is ultimately exported from tidal wetland soils and sediments (Ziegler and Benner, 1999; Bertilsson and Jones, 2003). Perhaps the least explored of these processes is the influence of DOC sorption-desorption on soil surfaces, a process that regulates DOC dynamics in upland forests and non-tidal wetlands (e.g. Qualls, 2000; Grybos et al., 2009) but remains largely unquantified in tidal wetland soils.

The sorption capacity of soils and sediments is strongly related to the content of poorly crystalline iron and aluminum oxides (citations). Poorly crystalline oxide surfaces have a high affinity for DOC, trace metals, silica, and phosphorus due primarily to their high specific surface area (Slomp et al., 1996; Kaiser and Guggenberger, 2000; Lalonde et al., 2012; Shields et al., 2016). As a result, poorly crystalline iron and aluminum oxide content is strong predictor of DOC sorption in both freshwater and marine sediments (citations) and well-drained terrestrial soils (Qualls, 2000; Guggenberger and Kaiser, 2003; Kaiser and Guggenberger, 2003; Wagai and Mayer, 2007; Kothawala and Moore, 2009; Kothawala et al., 2009, 2012). Studies of mineral-organic associations in wetlands number far fewer compared to those in terrestrial systems, but are known to play a significant role in the fractionation of nitrogen bound in DOC (Aufdenkampe et al., 2001), and the release of dissolved organic matter via reductive dissolution of manganese and Fe oxyhydroxides in non-tidal wetlands (Grybos et al., 2009). Due to the compositional heterogeneity of DOC (Thurman et al., 1985), and the poorly defined solubilities and surface characteristics of poorly crystalline metal oxides, the DOC affinity for metal oxide surfaces varies greatly (McKnight et al., 1992). However, the unique sorption mechanisms that are expected to operate in tidal wetland ecosystems where salinity is variable and rapidly changing remains largely unexplored and poorly understood.

The salinity environment of coastal wetlands is changing with sea level rise, with myriad and complex effects on carbon biogeochemistry. Increasing salinity is associated with decreases in soil carbon content, decreased inorganic nitrogen removal, and enhanced generation of sulfides (Herbert et al., 2015), and lower methane emissions (Poffenbarger et al., 2011). The resulting increased ionic strength can also block or displace ions from soil exchange sites (Seitzinger et al. 1991; Stumm and Morgan, 2012), and alter thermodynamic activity coefficients, leading to the dissolution of soil minerals such as iron (Baldwin et al., 2006). Thus, any research into DOC sorption dynamics in tidal wetlands should account for variations in salinity.

The objective of our study was to ascertain the dominant regulators of DOC exchange across tidal marshes that vary in salinity regime (freshwater to mixoeuhaline) and soil organic carbon content (mineral-dominated soils to highly organic soils). Based on the high specific surface area and reactivity of poorly crystalline iron (PC-Fe) and aluminum (PC-Al) minerals (e.g. McKnight et al. 1992; Kaiser and Guggenberger, 2000), and the role of ionic strength in blocking and displacing ions from reactive exchange sites at the mineral soil surface (Seitzinger et al. 1991; Stumm and Morgan, 2012), we hypothesized that the variability in the DOC sorption capacity would increase with mineral content and decrease with salinity. The results of this work will ultimately be used to inform the development of a novel coupled hydrodynamic-photo-biogeochemical coastal wetlands model, the Finite Volume Community Ocean Model – Integrated Compartment Model (FVCOM-ICM; Clark et al., 2018), for wetland-estuarine interfaces.

Methods

Soil Samples

We tested our hypothesis by examining the relationship between tidal marsh sediment composition, salinity environment, and dissolved organic carbon (DOC) concentration. Our study sites were selected based on salinity environment, soil organic carbon content, and the specific surface area of the soil mineral component. Soil cores, 0 – 40 cm, were collected using a gouge corer between March 5 and March 15, 2018 from four tidal marshes in Chesapeake Bay, USA: (i) Kirkpatrick Marsh in Edgewater, Maryland, USA (home of the Global Change Research Wetland (GCReW), 36°53'N, 76°33'W), (ii) Jug Bay Wetlands Sanctuary in Lothian, Maryland, USA (38°46'N, 76°42'W), (iii) Taskinas Marsh in Williamsburg, Virginia, USA (37°25'N, 76°43'W), and (iv) Wachapreague Marsh in Wachapreague, Virginia, USA (37°32'N, 75°41'W) (Fig. 1, Table 1). Surface vegetation was carefully cut away and the soil cores were manually cut into 5 cm segments for the top 10 cm of the core, and then into 10 cm segments for the remaining 30 cm of the core, before being individually bagged and transported back to the lab on ice where they were immediately frozen at -80°C. Two separate cores were taken from each wetland for bulk density determination and particle size analysis (PSA). These cores were treated as described above with the exception that they were stored at 4°C for no more than 24 hours prior to sample processing.

Bulk density was determined as per Blake and Hartge (1986) in which pre-weighed soil core segments of known length and diameter were oven-dried at 105°C for 72 hours and re-weighed. Soil core segments for PSA were treated based on a method modified from Zobeck (2004) where soils were air-dried for two weeks and passed through a 1 mm mesh test sieve. The frozen core segments were dried in a Labconco console freeze-dryer, passed through a 1 mm mesh test sieve, and combined into bulk samples by depth increment and site. Subsamples were taken from each freeze-dried depth increment bulk sample for %SOM, percent total organic

carbon (%TOC), specific surface area (SSA), poorly crystalline iron [PC-Fe], and poorly crystalline aluminum [PC-Al] determination before the depth-increment bulk samples for each site were combined to form the four bulk soil samples (0 – 40 cm) used in the sorption incubation experiment. Processed soil samples were stored in desiccators for the duration of this study.

SOM fraction was determined in triplicate via loss on ignition at 450°C for 24 hours using triplicate 2 g subsamples of freeze-dried soil (Heiri et al., 2001). % TOC was determined following the methods described in Hedges and Stern (1984). Small subsamples (1 - 15 mg) of freeze-dried soil were fumigated overnight with 6N HCl, dried, and packaged prior to analysis with a Carlo Erba Elemental Analyzer. Replicate analyses (n = 2 to 4) were run for all samples and the analytical variability was less than 5%. Prior to analysis for specific surface area and particle size, dried soils (0.6 to 1.0 g) were combusted for 12 hours at 350°C to remove organic material. Samples for specific area were degassed at 250°C for 2 hours on a Micrometric Flow Prep 060 to remove water. Soils were then analyzed by nitrogen adsorption using a 5-point BET method with a Gemini V Surface Area Analyzer. Combusted samples analyzed for particle size were measured in triplicate with a Beckman Coulter LS 13320 Laser Diffraction Particle Size Analyzer. Determination of [PC-Al] and [PC-Fe] was based on methods described in Kostka and Luther (1994) where triplicate samples of 0.3 g of freeze-dried soil were treated with 30 mL of degassed 0.5M HCl under anaerobic conditions, shaken on a horizontal shaker at 150 RPM for 1 hour, and then centrifuged at 4700 G for 1 hour. 20 mL of the supernatant was treated with 200 µL of 6M HCl and analyzed with an Agilent Technologies 7900 inductively coupled plasma mass spectrometer.

Dissolved Organic Carbon

In April 2018, approximately 115 L of surface water was collected in acid-washed carboys from the Jericho Ditch (36°41'45.03"N, 76°30'28.16"W) in the Great Dismal Swamp National Wildlife Refuge (GDS), a non-tidal forested wetland located on the coastal plain of southeastern Virginia and northeastern North Carolina, USA (36°37'N, 76°28'W; Fig. 1). The carboys were transported surrounded by bagged ice and covered with a thick tarp to prevent DOC photodegradation. Samples were stored at 4°C in the dark for no more than 24 hours prior to sample processing.

The DOC in 115 L of Jericho ditch water was concentrated by reverse osmosis (RO) using a Growonix GX600 RO-system fitted with both pleated and spun sediment filters. The retentate was cycled back into the sample carboy, which was topped off with fresh sample as volume decreased, and the purified water was discarded except for a subsample that was kept for DOC determination. The DOC concentrate was passed through a 20 μm-pore size Whatman Polycap 75 HD disposable filter capsule followed by a 0.2 μm-pore size Whatman Polycap 36 TC polyethersulfone membrane capsule before being stored at 4°C in the dark. The concentrate was then treated with enough sodium azide (NaN_3), a microbial inhibitor, to obtain a final concentration of 1 mM NaN_3. DOC concentration ([DOC]) was measured on a Shimadzu TOC-L using high-temperature combustion.

Batch Incubations

The treated DOC concentrate had a [DOC] of 217 mg-DOC L^{-1}, a pH of 4.40, a salinity of 0.08 mg g^{-1}, and a specific conductivity of 180 μS cm^{-1}. This stock was portioned off into four sub-stocks and instant ocean aquarium salt was added to three of the stocks to produce salinities of 0 psu (no instant ocean added), 10 psu, 20 psu, and 35 psu. Each of these stocks were used to prepare 7 'isotherm standards' ranging in [DOC] from 0 to ~ 200 mg L^{-1} by dilution with a

179 "zero" DOC solution (< 0.2 mg-DOC L-1; hereafter referred to as the dilutant) of similar pH,
180 salinity, and specific conductivity prepared with ultrapure water, instant ocean aquarium salt, 1
181 mM NaN_3, and dilute HCl. Isotherm standards were freshly prepared for each batch incubation.
182 The batch incubations were performed based on methods described by Kothawala et al.
183 (2008) under a 95% nitrogen (N_2) and 5% hydrogen (H_2) atmosphere in a Coy Laboratory
184 Products anaerobic chamber using solutions degassed with N_2. 30 mL of isotherm standard was
185 added to triplicate samples of 1 g soil in 50 mL centrifuge tubes, capped, wrapped in aluminum
186 foil, and laid flat in a horizontal shaker for 24 hours at room temperature (~22°C) at a speed of
187 70 RPM. The samples were then centrifuged at 4700 g for 1 hour, the supernatant decanted, and
188 both salinity (WTW Multi 340i probe) and pH (Thermo Orion 3 Star pH meter) measured before
189 the supernatant was syringe-filtered using disposable 0.45 µm Millex filter cartridges. Potential
190 DOC contribution from the filter cartridges was avoided by discarding the first few milliliters of
191 the filtrate for each sample.
192 *Sorption Isotherms*
193 The traditional Langmuir isotherm (Eq. 1) accounts for the desorption of native adsorbed
194 organic carbon (C_0) and expresses a relationship between the quantity of DOC adsorbed
195 ($\Delta[DOC]_{0\text{-}f}$) in mg-DOC g^{-1}, the final DOC concentration ($[DOC]_f$) in mg-DOC L^{-1}, the bulk
196 DOC binding affinity (K) in L g^{-1}, and the maximum adsorption capacity (Q_{max}) in mg-DOC g^{-1}
197 (Kothawala et al., 2008).
198 $$\Delta[DOC]_{0-f} = \frac{(Q_{max} * K * [DOC]_f)}{(1+(K*[DOC]_f))} - C_0 \qquad (1)$$
199 The Langmuir isotherm parameters, Q_{max}, C_0, and K, were derived by fitting the $\Delta[DOC]_{0\text{-}f}$ vs.
200 $\Delta[DOC]_f$ data using non-linear regression as per Equation 1. Due to the almost linear fit of the
201 isotherms for Taskinas and GCReW in the 35 psu salinity incubations, the Q_{max} for these

isotherms were anomalously large and had a very large standard error, suggesting that a wide range of Q_{max} values would be an appropriate fit for the regression line. Consequently, the relationship between Q_{max} and salinity for both GCReW and Taskinas soils was assumed to be linear and the Q_{max} values derived for the 0, 10, and 20 psu salinity treatments were used to extrapolate the Q_{max} values at 35 psu using the TREND function in Microsoft Excel. The TREND function calculates a linear trend given a series of dependent (y) and independent (x) variables and returns values along that trend line. Though the extrapolated Q_{max} values reported fell within the range predicted by the non-linear regression, these two values were omitted from statistical analysis.

The null point is defined as the equilibrium concentration at which there is no net removal (adsorption) or release (desorption) of DOC from solution, the biogeochemical significance of which is… It is calculated as the x-intercept of the fitted isotherm curves (Vandenbruwane et al., 2007), was calculated for each isotherm as the $[DOC]_f$ where $\Delta[DOC]_{0\text{-}f}$ = 0 mg-DOC g^{-1} as per equation 2.

$$NP = \frac{C_0}{((Q_{max} - C_0) * K)} \qquad (2)$$

Any statistics involving the NP omitted values for the 35 psu salinity treatment of the GCReW and Taskinas sites.

Statistics

Statistics were conducted using SigmaPlot 12.3, JMP 14.0, and RStudio 1.2.5033. Normality of the dataset, or residuals in the case of multiple regression, was tested using the Shapiro-Wilk test, and homoscedasticity was determined using Levene's test. In the case of normality and equal variance, analysis of variance (ANOVA) with post hoc Tukey Honest Significant Difference test (Tukey HSD) was used to test for differences in group means.

Stepwise regression was used to identify soil composition predictors for soil specific surface area, multiple linear regression analysis was used to test the significance of the relationship, and studentized residuals were used to identify regression outliers. Linear mixed effect models (Table S1) were used to determine the relationship between Qmax, salinity, and [PC-Fe] and between K and salinity with site as the random variable with the r^2 calculated using 'piecewiseSEM' package in RStudio (Lefcheck, 2016). In the case of unequal variance or when normality was not successfully obtained using log transformation, Kruskal–Wallis with post-hoc Steel-Dwass was used to compare groups, Wilcoxon Ranked Sums to compare pairs, and Spearman correlations were used. Error estimates presented in this paper are standard error unless otherwise specified. Analyses were conducted on data derived from bulk soil samples unless otherwise specified.

Results

Soil characterization

The four locations in our study were selected to represent a wide range of characteristics expected to influence dissolved organic carbon (DOC) sorption dynamics. The GCReW site had the highest soil organic matter (SOM) and total organic carbon (TOC) content (75% and 35%, respectively) and consequently the lowest bulk density (0.11 g cm^{-3}) (Table 1). The Wachapreague site was lowest in SOM and TOC (5% and 2%, respectively) and highest in bulk density (1.99 g cm^{-3}), and therefore had the most sand, silt, and clay of the four sites per volume (i.e. g cm^{-3}; Table 1). Except for the Wachapreague soil, the %TOC, %SOM, and bulk density reported here are comparable to the ranges of 3.1% to 48.3%, 5.80% – 87.9 %, and 0.040 to 0.846 g cm^{-3}, respectively, reported by Williams and Rosenheim (2015) for freshwater and salt marshes and by Neubauer (2008) for tidal marsh soils along the Atlantic coast of the United

States. Though the Wachapreague soil exhibited significantly higher bulk density than the other three marsh soils by a factor of ~ 6.5 due to its predominantly mineral makeup, the results were comparable to the soil bulk densities > 1.5 g cm^{-3} previously measured at that site (L. Schile-Beers, unpublished data).

The variation in specific surface area (SSA), poorly crystalline iron content ([PC-Fe]), and poorly crystalline aluminum content ([PC-Al]) amongst our four tidal wetland soils highlights the wide range of mineralogy represented by these sites. These three mineralogical characteristics were independent of the percent mineral matter in the soil (i.e. 100 - %SOM). SSA and [PC-Fe] were greatest at the Jug Bay site, 41 m^2 g^{-1} and 11 g g^{-1}, respectively, while [PC-Al] was greatest at the Taskinas site (1.5 mg g^{-1}). SSA was lowest at the Wachapreague site (7 m^2 g^{-1}) while both [PC-Fe] and [PC-Al] were lowest at the highly organic GCReW site (Table 1). This range of poorly crystalline mineral content fell within the range of ~0.1 to 4.5 mg-Fe g-$soil^{-1}$ and ~0.3 to 1.6 mg-Al g-$soil^{-1}$ reported by Marton and Roberts (2014) for Louisiana salt marsh soils with the exception of the Jug Bay soil which contained substantially greater [PC-Fe]. However, similar to our result of 11.2 ± 1.7 mg-Fe g-$soil^{-1}$, previous soil analyses conducted at Jug Bay by Keller et al. (2013) reported [PC-Fe] of ~10 mg-Fe g-$soil^{-1}$ thereby validating our result. SSA, [PC-Al], and [PC-Fe] all differed significantly among the four soils ($F_{3,10} = 45.4$, $p < 0.001$, Tukey HSD ≤ 0.0431, $chi^2(3) = 47.6$, $p < 0.0001$, and $chi^2(3) = 45.2$, $p < 0.0001$, Steel-Dwass $p \leq 0.0004$) with the following exceptions: SSA did not differ significantly between GCReW and Wachapreague ($p = 0.055$), [PC-Al] did not differ significantly between Taskinas and Wachapreague soils ($p = 0.072$), and [PC-Fe] did not differ significantly between Wachapreague and Taskinas soils ($p = 0.971$). Multiple linear regression results suggested that

[PC-Al] and [PC-Fe] explained 84% of the variability in mineral SSA (r^2_{adj} = 0.844, $F_{2,1}$ = 36.2, p < 0.0001, Std β_{Al} = 0.440, Std β_{Fe} = 0.703; Table S2).

The mineral phase particle size distribution of the GCReW, Jug Bay, and Wachapreague soils corresponded to that of a silty loam while that of the Taskinas soil corresponded to a loam (Liebens, 2001), two soil textures commonly found in coastal wetlands (Lyu et al., 2015; Pellegrini et al., 2018). Despite significant differences in mineralogy, the sand, silt, and clay fractions did not differ significantly amongst the four sites (p = 0.15 – 0.47) nor were there any significant correlations between any of these particle size fractions and either SSA or poorly crystalline mineral content (p > 0.342, not shown). Mean %sand, %silt, and %clay differed by no more than 14%, 19%, and 5%, respectively, across all four sites (Table 1).

The initial pH of the four degassed Great Dismal Swamp DOC stocks used to prepare the isotherm standards was 4.60 ± 0.09. Post-incubation pH increased significantly in all batch incubations with GCReW, Taskinas, Jug Bay, and Wachapreague yielding final pH values of 6.74 ± 0.03, 6.66 ± 0.04, 5.16 ± 0.05, and 6.94 ± 0.10, respectively, resulting in ΔpH of 1.96 ± 0.06, 1.87 ± 0.06, 0.37 ± 0.06, and 2.18 ± 0.10, respectively. ΔpH showed a significant negative correlation with soil [PC-Fe] (Spearman *ρ* = -0.622, p < 0.0001, not shown), however, Δsalinity did not exceed 2.5 psu in any of the soil incubations in this study. Incubations without soil were performed at 12.5 mg-DOC L^{-1} and 285 mg-DOC L^{-1} across the four salinity treatments, but there were no significant differences in [DOC] between any of the pre- and post-incubation pairings ($chi^2(1) = 4.76 \times 10^{-2}$ to 2.33, p > 0.1, Fig. S1), suggesting that there is no precipitation of DOC in the absence of soil in our experiments.

Langmuir sorption isotherms

The sorption isotherm plots for all four marsh soils are presented in Fig. 2 and the sorption characteristics calculated using the traditional Langmuir isotherm approach are presented in Table 2. The lowest r^2 of the non-linear regressions performed to fit the Langmuir isotherms for all soils across the four salinity treatments was 0.889 with a mean of 0.974 ± 0.007. For each individual soil, the maximum adsorption capacity (Q_{max}) generally increased with salinity, the DOC binding affinity (K) and null point (NP) tended to generally decrease with salinity, and native adsorbed organic carbon (C_0) showed no consistent trend in response to salinity. The low SSA Wachapreague soils consistently yielded the lowest Q_{max} and C_0 across all salinity treatments with Q_{max} ranging between approx. 3 and 5 mg-C g-soil^{-1} in the 0 psu and 35 psu salinity treatments, respectively, and a mean C_0 of $3.46 \times 10^{-1} \pm 3.45 \times 10^{-2}$ mg-C g^{-1} (standard deviation). The high SSA, iron-rich Jug Bay soil, on the other hand, consistently yielded the greatest Q_{max} and C_0 across all salinity treatments, with Q_{max} ranging between approx. 6 and 13 mg-C g-soil^{-1} in the 0 psu and 35 psu salinity treatments, respectively, and a mean C_0 of $4.40 \pm 1.15 \times 10^{-1}$ mg-C g-soil^{-1} (standard deviation).

The mineral Wachapreague soil incubations also yielded the lowest NP across all salinity treatments, ranging from 192 mg-DOC L^{-1} to 40.1 mg-DOC L^{-1} in the 0 psu and 35 psu salinity treatments, respectively, and the organic-rich GCReW soil incubations yielded the greatest NP, ranging from 2250 mg-DOC L^{-1} to 114 mg-DOC L^{-1} in the 0 psu and 35 psu salinity treatments, respectively (Table 2). Though K tended to decrease with greater salinity for each individual soil, the soil with the greatest and least K values did not remain consistent across the salinity treatments. The Jug Bay soil incubation yielded the highest K in the 0 psu treatment and the Taskinas soil incubation yielded the lowest K in the 35 psu salinity treatment with values of $1.08 \times 10^{-2} \pm 3.08 \times 10^{-3}$ L g^{-1} and $3.45 \times 10^{-2} \pm 9.60 \times 10^{-3}$ L g^{-1}, respectively.

315 Linear mixed effect modelling results (Table 3) suggest that 64% of the variability in
316 Q_{max} can be explained by fixed effects only (salinity, [PC-Fe], and the interaction between
317 salinity and PC-Fe; $p \leq 0.0473$) though [PC-Fe] by itself was not a significant predictor ($p =$
318 0.233). This explained variability in Q_{max} increased to 92% when both fixed and random (site)
319 effects were included. Meanwhile, 80% of the variability in K was explained by salinity alone
320 with random effects (site) included (Table 4; $p = 0.0005$). Though [PC-Fe] was not a significant
321 predictor for K in the linear mixed effect model, the two correlated positively and significantly
322 (Spearman p = p = 0.546, p = 0.0288; Figure 3a). Similarly, C_0 correlated positively with SSA
323 (Spearman p = 0.837, $p < 0.0001$; Figure 3b) and the NP correlated positively with %TOC
324 (Spearman p = 0.667, $p < 0.0001$, Fig. 3c).

325 **Discussion**

326 Previous research on the sorption of solutes within soils has focused on terrestrial and
327 non-tidal wetland ecosystems; our study expands on this body of work by assessing the
328 partitioning of dissolved organic carbon (DOC) in disparate soils from four coastal tidal wetlands
329 across a range of salinities and establishing relationships between sorption characteristics and
330 key soil properties using traditional Langmuir isotherms. Our main finding suggests that, though
331 both the maximum soil sorption capacity (Q_{max}) and DOC bonding affinity (K) play key roles in
332 sorption at the soil surface, changes in salinity influence the two differently with greater salinity
333 increasing the soil sorption capacity but decreasing K. The enhancement of Q_{max} with salinity
334 was somewhat mitigated in wetland soils with greater poorly crystalline iron content ([PC-Fe])
335 though [PC-Fe] alone was not a significant predictor of Q_{max}. These findings support our
336 hypothesis that the variability in the quantity of DOC exchanged in tidal marsh soils is mainly a

function of soil type and salinity and provide much-needed elucidation of the mechanisms of DOC exchange at the tidal marsh-estuarine interface.

Soil Texture

The lack of significant difference in particle size distribution amongst our four wetland soils may be due to collecting our soil cores from high marsh locations ≥ 20 m from their respective tidal creek banks. Previous studies have reported that clays play a significant role in DOC sorption through their high surface area and charged surfaces (Kiel et al., 1994; Guggenberger and Kaiser, 2003). Suspended sediment particle size distribution tends to shift towards smaller, lighter particles such as clays with greater distance from the tidal creek as coarser, heavier sediments brought in with the flooding tide either settle out or are intercepted by surface vegetation (Moskalski and Sommerfield, 2012). As such, it is possible that particle size plays a more significant role in DOC sorption in soils that are in closer proximity to a tidal creek. However, Moskalski and Sommerfield found that that the vast majority of suspended sediment concentration decrease occurred within ~5 m of the tidal creek edge in a Delaware salt marsh. Consequently, as the marsh-area resolution in the FVCOM-ICM model is 10 m (Clark et al., 2018), larger than the near-creek area where the coarsest and heaviest particles are likely to settle or be intercepted, we do not expect the potential contribution of particle size relative to that of poorly crystalline hydrous Fe and Al oxides to affect our ability to apply our sorption results to model processes right at the wetland-tidal creek interface. However, future fieldwork and model development should certainly include more spatially heterogeneous sorption measurements to account for differences in sediment deposition.

Sorption Isotherms

359 Kaiser and Guggenberger (2003) found that mineralogy controlled the relationship
360 between specific surface area (SSA) and the sorption of organic matter in forest soils. The
361 significant, positive relationship between both poorly crystalline iron content ([PC-Fe]) and
362 poorly crystalline aluminum content ([PC-Al]) and SSA (Table S2), and a similar relationship
363 between [PC-Fe] and the maximum soil sorption capacity (Q_{max}) (Table 3) suggest the DOC
364 sorption in tidal marsh soils operates by similar mineralogical mechanisms. The significant
365 positive correlations between DOC binding affinity (K) and [PC-Fe] as well as between the
366 quantity of initial soil exchangeable carbon (C_0) and SSA also suggest that soils richer in poorly
367 crystalline minerals, and, thus, with greater SSA, hosted a greater pool of natively-sorbed DOC.
368 The correlation between [PC-Fe], and the lack of correlation with [PC-Al], on DOC binding
369 affinity might stem from binding competition between Al and Fe for humic substances (Tipping
370 et al. 2002), a major component of wetland DOC (Tzortziou et al., 2008; Watanabe et al., 2012),
371 as humic acid binding affinities have been reported to be six times greater for Fe relative to Al
372 (Bhandari et al., 1999).
373 *Impact of Salinity on Sorption Isotherms*
374 Differences in salinity had a substantial impact on both Q_{max} and DOC binding affinity
375 (K), though the respective impact on each is notably different. The increase in Q_{max} with greater
376 salinity observed in our four tidal marsh soils was likely due to the direct ionic displacement of
377 natively-sorbed DOC (Kalbitz, 2000). The decrease in K with greater salinity may stem from
378 ionic strength-induced changes to dissolved humic structural conformation, essentially the 3-D
379 shape of the humic compounds. At high ionic strength, the charge repulsion between adjacent
380 hydroxyl and carbonyl groups is neutralized resulting in the humic substance adopting a coiled
381 conformation or shape (Baalousha et al. 2006; Tsutsuki and Kuwatsuka, 1984) which, at the

382 mineral surface, could result in fewer available attachment points (Tipping and Cooke, 1982).
383 Consequently, our results suggest that, though rising salinity may increase the number of
384 potential sorption sites on the soil surface, it may decrease the ability of complex DOC
385 compounds such as humic acids to bind to those sites. At low solute concentrations, these
386 salinity effects have similar magnitudes, but operate in opposing directions, on sorption, such
387 that their net effect is minimal (cf. Fig. 2). At high solute concentrations, Q_{max} has the dominant
388 influence so that sorption increases with salinity. Therefore, the influence of increased salinity on
389 sorption processes in tidal marsh soils, and ultimately tidal marsh carbon export to estuarine
390 waters, will interact with salinity-induced changes in [DOC].

391 Unlike Kothawala et al. (2009), we did not find a relationship between the null point
392 (NP) and a combination of TOC and poorly crystalline mineralogy but only a positive correlation
393 between TOC and the NP. A multiple linear regression of the NP vs [PC-Al] and [PC-Fe] in our
394 data yielded a similar r^2, 0.3, to the 0.33 reported by Kothawala et al. (2009), but our regression
395 residuals did not meet statistical assumptions of normality and equal variance. This might be due
396 to our comparatively small sample size where we only analyzed four distinct soils compared to
397 the 52 soils analyzed by Kothawala et al. (2009). The correlation between TOC and the NP in
398 our data, however, does support their findings that the organic carbon content of the soil
399 influences the balance between adsorption and desorption of DOC.

400 Though quantifying the contribution of organic-organic sorption relative to mineral-
401 organic sorption was outside the scope of this study, it is likely that cation and water-bridging, as
402 well as the aforementioned H-bonding and van der Waals forces (Bolan et al., 2011), are
403 important mechanisms in very organic tidal march soils such as those found at GCReW (~75%
404 SOM), where the ratio of [PC-Al + Fe]:TOC was found to be an order of magnitude lower than

405 the other three soils. SOM contains a variety of functional groups that vary in polarity, such as
406 anionic hydroxyls, uncharged aromatic moieties, and cationic amino groups. Consequently, in
407 addition to soil mineralogy, the variation in abundance of these groups, SSA, and the chemical
408 composition of SOM has the potential to significantly influence soil sorption characteristics
409 (Johnston and Tombácz, 2002) and needs further study.

410 Similar to the increase in pH reported by Kothawala et al. (2009) in their sorption
411 incubations of soils from volcanic B soil horizons, we observed an increase in pH in all our
412 incubations, most notably in the GCReW, Taskinas, and Wachapreague soils. This supports
413 ligand exchange as the dominant sorption mechanism in our soils as hydroxyl groups, which are
414 coordinated to metal ions like Al and Fe on the soil surface, are replaced by organic ligands to
415 form a surface complex; the release of these hydroxyl groups result in an increase in solution pH
416 (McKnight et al., 1992). The comparatively small change in solution pH in Jug Bay incubations
417 relative to the other three soils suggests that Jug Bay soils are relatively low in base saturation, a
418 condition that is consistent with the fresh, low alkalinity setting of this site, and the observation
419 that it was the only site with a negative correlation between ΔpH and [PC-Fe].

420 It is possible that there was some dissolution of soil iron minerals due to the low initial
421 pH of our DOC isotherm standards (~4.6) and high salinity in some of our treatments. However,
422 due to the use of NaN_3 and conducting our experiments under anaerobic conditions, any
423 dissolution would be chemical and not biotic and Fe^{3+} would be reduced to Fe^{2+} to which DOC
424 has a much lower affinity for complexation (Riedel et al., 2013). The contribution of dissolution
425 to the overall DOC removal from solution is further minimized by all four soils undergoing
426 identical treatment and being compared only to one another. Elucidating the relative

427 contributions of both sorption and complexation/precipitation to organo-mineral interactions in
428 tidal marsh soils warrants further research.

429 **Implications for Modeling Sea Level Rise**

430 Solute exchange at the soil surface has been extensively studied in terrestrial and non-
431 tidal wetland ecosystems, and it is well established that there is transformation and exchange of
432 dissolved organic carbon (DOC) at the tidal-estuarine interface. However, there remains a dearth
433 of knowledge on the behavior of DOC in tidal wetland soils, and on the influence of soils on the
434 amount and composition of DOC exchanged at the soil surface. The lack of mechanistic
435 knowledge on DOC interactions with soils limits our ability to model marsh-estuarine carbon
436 exchange using estuarine or Earth System Models, and to forecast the impacts of sea level rise,
437 or other extreme or compounding disturbances impacting marsh soil characteristics, on carbon
438 cycles at the terrestrial-aquatic interface (DOE, 2017). Our study demonstrates that salinity and
439 poorly crystalline iron are important abiotic controls on sorption processes in tidal wetlands.
440 These parameters are commonly resolved in spatial databases and observational datasets,
441 suggesting that forecast models could be refined to account for interactions between soil surfaces
442 and DOC.

443 Tidal brackish and salt marshes are routinely exposed to salinity regimes that range from
444 mesohaline to mixoeuhaline, while tidal freshwater marshes are routinely exposed to waters of <
445 0.5 psu. Salinity is increasing in coastal wetlands experiencing rising sea levels (Wigley, 2005),
446 though patterns of salinity change are complex due to the influence of factors such as changes in
447 precipitation in the watersheds of rivers (Smith et al., 2005) and freshwater withdrawal
448 (Hamilton, 1990; Knowles, 2002). Our findings that increases in salinity influence soils sorption
449 capacity and DOC binding affinity in opposing ways suggests that tidal marshes may be

exhibiting complex physicochemical responses to increased salinity, with the balance between carbon sequestration (sorption) and mobilization (desorption) depending on the [DOC]. Further research into these sorption controls at greater soil depths and with more spatial variation will be instrumental in improving our understanding of tidal wetland sorption dynamics, and our ability to predict their responses to anthropogenic disturbances and global climate change.

Acknowledgements

We would like to thank the staff of the Jug Bay Wetlands Sanctuary, the York River State Park, the Virginia Institute of Marine Science (VIMS) Eastern Shore Laboratory, and the Great Dismal Swamp National Wildlife Refuge for their support and assistance. In particular, we are grateful to Amanda Knobloch, Yanhua Feng, and Sean Fate (VIMS), Willy Reay (Chesapeake Bay National Estuarine Research Reserve), Michael Gonsior (University of Maryland Center for Environmental Science, Chesapeake Biological Laboratory), Jade Dominique Walker (University of Maryland University College), Ellen Weber (Wilkes University), and Andrew Peresta (Smithsonian Environmental Research Center) for their assistance in the field and laboratory. This study was funded by National Science Foundation grant DEB-1556556; NASA grant NNX14AP06G; NSF-LTREB Program support of the Global Change Research Wetland (DEB-0950080, DEB-1457100, DEB-1557009); and the Smithsonian Environmental Research Center. This paper is Contribution No.xxxx of the Virginia Institute of Marine Science, William & Mary.

References and Citations

Aufdenkampe, A. K., J. I. Hedges, J. E. Richey, A. V. Krusche, and C. A. Llerena. 2001. Sorptive fractionation of dissolved organic nitrogen and amino acids onto fine sediments

473 within the Amazon Basin. *Limnol. Oceanogr. 46*(8): 1921-1935,
474 doi:10.4319/lo.2001.46.8.1921
475 Baalousha, M., M. Motelica-Heino, and P. L. Coustumer. 2006. Conformation and size of humic
476 substances: Effects of major cation concentration and type, pH, salinity, and residence
477 time. *Colloids Surf A Physicochem Eng Asp* 272(1): 48-55, doi:
478 10.1016/j.colsurfa.2005.07.010
479 Baldwin, D. S., G. N. Rees, A. M. Mitchell, G. Watson, J. Williams. 2006. The short-term
480 effects of salinization on anaerobic nutrient cycling and microbial community structure in
481 sediment from a freshwater wetland. *Wetlands 26*(2): 455-464, doi:10.1672/0277-
482 5212(2006)26[455:tseoso]2.0.co;2
483 Bertilsson, S., and J. B. Jones. 2003. 1 - Supply of dissolved organic matter to aquatic
484 ecosystems: Autochthonous sources. In S. E. G. Findlay & R. L. Sinsabaugh (Eds.),
485 *Aquatic Ecosystems,* 3-24, Burlington: Academic Press.
486 Bhandari S. A. D. Amarasiriwardena, and B. Xing. 1999. Application of high performance size
487 exclusion chromatography (HPSEC) with detection by inductively coupled plasma-mass
488 spectrometry (ICP-MS) for the study of metal complexation properties of soil derived
489 humic acid molecular fractions. In G. Davies, E. A. Ghabbour (Eds.) *Humic Substances:*
490 *Advanced Methods, Properties, and Applications*. Royal Society of Chemistry:
491 Cambridge.
492 Blake, G. R., and K. H. Hartge. 1986. Bulk density. In A. Klute (Ed.), *Methods of Soil Analysis:*
493 *Part 1—Physical and Mineralogical Methods,* 363-375. Madison, WI: Soil Science
494 Society of America, American Society of Agronomy.

Bolan, N. S., D. C. Adriano, A. Kunhikrishnan, T. James, R. McDowell, and N. Senesi. 2011. Chapter One - Dissolved Organic Matter: Biogeochemistry, Dynamics, and Environmental Significance in Soils. In D. L. Sparks (Ed.), *Advances in Agronomy* 110: 1-75), Academic Press, doi: 10.1016/B978-0-12-385531-2.00001-3

Brady, N. C., and R. R. Weil. 2009. *Elements of the Nature and Properties of Soils*. New Jersey: Prentice Hall

Childers, D. L., J. W. Day Jr., and H. N. McKellar Jr. 2000.Twenty more years of marsh and estuarine flux studies: Revisiting Nixon (1980). In: Weinstein, M. and D. A. Kreeger (eds.). *Concepts and Controversies in Tidal Marsh Ecology*. Kluer Academic Publishing: Dordecht, Netherlands.

Clark, C. D., L. P. Litz, and S. B. Grant, 2008. Saltmarshes as a source of chromophoric dissolved organic matter (CDOM) to Southern California coastal waters, *Limnol. Oceanogr*: 53(5): 1923-1933, doi: 10.4319/lo.2008.53.5.1923.

Clark, J. B., W. Long, M. Tzortziou, P. J. Neale, and R. R. Hood. 2018. Wind-driven dissolved organic matter dynamics in a Chesapeake Bay tidal marsh-estuary system. *Estuaries Coast 41*(3): 708-723, doi:10.1007/s12237-017-0295-1

Davis, J. A. 1982. Adsorption of natural dissolved organic matter at the oxide/water interface. Geochim Cosmochim Acta, 46(11): 2381-2393. doi:https://doi.org/10.1016/0016-7037(82)90209-5.

Google Earth Pro V 7.3.2.5776. March 1, 2019. Chesapeake Bay, USA, 37°50'25.59" N, 76°09'25.01" W, Eye alt 442 m.

516 Grybos, M., M. Davranche, G. Gruau, P. Petitjean, and M. Pédrot. 2009. Increasing pH drives
517 organic matter solubilization from wetland soils under reducing conditions. *Geoderma*
518 *154*(1-2): 13-19, doi:10.1016/j.geoderma.2009.09.001
519 Guggenberger, G., and K. Kaiser. 2003. Dissolved organic matter in soil: Challenging the
520 paradigm of sorptive preservation. *Geoderma 113*(3-4): 293-310, doi:10.1016/s0016-
521 7061(02)00366-x
522 Hamilton, P. 1990. Modeling salinity and circulation for the Columbia River Estuary, P*rog.*
523 *Oceanogr. 25*: 113– 156. doi: 10.1016/0079-6611(90)90005-M
524 Hansen, A. M., T. E. C. Kraus, B. A. Pellerin, J. A. Fleck, B. D. Downing, and B. A.
525 Bergamaschi. 2016. Optical properties of dissolved organic matter (DOM): Effects of
526 biological and photolytic degradation. *Limnol. Oceanogr. 61*(3): 1015-1032.
527 doi:10.1002/lno.10270
528 Hedges, J. I., and J. H. Stern, 1984. Carbon and nitrogen determinations of carbonate-containing
529 solids. *Limnol. Oceanogr. 29*(3): 657-663, doi:10.4319/lo.1984.29.3.0657
530 Heiri, O., A. F. Lotter, and G. Lemcke. 2001. Loss on ignition as a method for estimating organic
531 and carbonate content in sediments: Reproducibility and comparability of results. *J.*
532 *Paleolimnol. 25*(1): 101-110, doi:10.1023/a:1008119611481
533 Herbert, E. R., P. Boon, A. J. Burgin, S. C. Neubauer, R. B. Franklin, M. Ardón, K. N.
534 Hopfensperger, L. P. M. Lamers, and P. Gell. 2015. A global perspective on wetland
535 salinization: ecological consequences of a growing threat to freshwater wetlands.
536 *Ecosphere 6*(10): art206, doi:10.1890/es14-00534.1
537 Herrmann, M., R. G. Najjar, W. M. Kemp, R. B. Alexander, E. W. Boyer, W.-J. Cai, P. C.
538 Griffith, K. D. Kroeger, S. L. McCallister, R. A. Smith. 2015. Net ecosystem production

539 and organic carbon balance of U.S. East Coast estuaries: A synthesis approach. *Global*
540 *Biogeochem. Cy. 29*(1): 96-111, doi:10.1002/2013gb004736
541 Johnston, C.T., and E. Tombácz. 2012. Surface chemistry of soil minerals. In J. B. Dixon, D. G.
542 Shulze (Eds.) *Soil Mineralogy With Environmental Applications.* Soil Science Society of
543 America: Madison, Wisconsin.
544 Kaiser, K., and G, Guggenberger. 2000. The role of DOM sorption to mineral surfaces in the
545 preservation of organic matter in soils. *Org. Geochem. 31*(7-8): 711-725,
546 doi:10.1016/s0146-6380(00)00046-2
547 Kaiser, K., and G. Guggenberger. 2003. Mineral surfaces and soil organic matter. *Eur. J. Soil*
548 *Sci. 54*(2): 219-236, doi:10.1046/j.1365-2389.2003.00544.x
549 Kalbitz, K., S. Solinger, J. H. Park, B. Michalzik, and E. Matzner. 2000. Controls on the
550 dynamics of dissolved organic matter in soils: A review. *Soil Science 165*(4): 277-304,
551 doi:10.1097/00010694-200004000-00001
552 Keil, R. G., E. Tsamakis, C. B. Fuh, J. C. Giddings, and J. I. Hedges. 1994. Mineralogical and
553 textural controls on the organic composition of coastal marine sediments: Hydrodynamic
554 separation using SPLITT-fractionation. *Geochim. Cosmochim. Acta 58*(2): 879-893, doi:
555 10.1016/0016-7037(94)90512-6
556 Keller, J. K., A. E. Sutton-Grier, A. L. Bullock, J. P. Megonigal. 2013. Anaerobic metabolism in
557 tidal freshwater wetlands: I. Plant removal effects on iron reduction and methanogenesis.
558 *Estuaries Coast 36*(3): 457-470, doi:10.1007/s12237-012-9527-6
559 Knowles, N. 2002. Natural and management influences on freshwater inflows and salinity in the
560 San Francisco Estuary at monthly to interannual scales. *Water Resour. Res. 38*(12): 1289,
561 doi:10.1029/2001WR000360

562 Kostka, J. E., and G. W. Luther. 1994. Partitioning and speciation of solid phase iron in
563 saltmarsh sediments. *Geochim. Cosmochim. Acta 58*(7): 1701-1710, doi: 10.1016/0016-
564 7037(94)90531-2
565 Kothawala, D. N., and T. R. Moore. 2009. Adsorption of dissolved nitrogen by forest mineral
566 soils. *Can. J. For. Res. 39*(12): 2381-2390, doi:10.1139/x09-147
567 Kothawala, D. N., T. R. Moore, and W. H. Hendershot. 2008. Adsorption of dissolved organic
568 carbon to mineral soils: A comparison of four isotherm approaches. *Geoderma 148*(1):
569 43-50, doi:10.1016/j.geoderma.2008.09.004
570 Kothawala, D. N., T. R. Moore, and W. H. Hendershot. 2009. Soil properties controlling the
571 adsorption of dissolved organic carbon to mineral soils. *Soil Sci. Soc. Am. J. 73*(6): 1831,
572 doi:10.2136/sssaj2008.0254
573 Kothawala, D. N., C. Roehm, C. Blodau, and T. R. Moore. 2012. Selective adsorption of
574 dissolved organic matter to mineral soils. *Geoderma 189-190*: 334-342,
575 doi:10.1016/j.geoderma.2012.07.001
576 Lalonde, K., A. Mucci, A. Ouellet, and Y. Gélinas. 2012. Preservation of organic matter in
577 sediments promoted by iron. *Nature 483*(7388): 198-200, doi:10.1038/nature10855
578 Lefcheck, J.S. 2016, piecewiseSEM: Piecewise structural equation modelling in r for ecology,
579 evolution, and systematics. Methods Ecol Evol, 7: 573-579. doi:10.1111/2041-
580 210X.12512.
581 Liebens, J. 2001. Spreadsheet macro to determine usda soil textural subclasses. *Commun. Soil*
582 *Sci. Plan. 32*(1-2): 255-265, doi:10.1081/CSS-100103005

583 Lyu, X., J. Yu, M. Zhou, B. Ma, G. Wang, C. Zhan, G. Han, B. Guan, H. Wu, Y. Li, D. Wang.
584 2015. Changes of soil particle size distribution in tidal flats in the Yellow River delta.
585 *Plos One 10*(3): e0121368, doi:10.1371/journal.pone.0121368
586 Maie, N., R. Jaffé, T. Miyoshi, and D. L. Childers. 2006. Quantitative and qualitative aspects of
587 dissolved organic carbon leached from senescent plants in an oligotrophic wetland.
588 *Biogeochemistry 78*(3): 285-314, doi:10.1007/s10533-005-4329-6
589 Marschner, B., and K. Kalbitz. 2003. Controls of bioavailability and biodegradability of
590 dissolved organic matter in soils. *Geoderma, 113*(3-4): 211-235, doi:10.1016/s0016-
591 7061(02)00362-2
592 Marton, J. M., and B. J. Roberts. 2014. Spatial variability of phosphorus sorption dynamics in
593 Louisiana salt marshes. *J. Geophys. Res. Biogeosci. 119*(3): 451-465,
594 doi:10.1002/2013jg002486
595 McKnight, D. M., K. E. Bencala, G. W. Zellweger, G. R. Aiken, G. L. Feder, and K. A. Thorn.
596 1992. Sorption of dissolved organic carbon by hydrous aluminum and iron oxides
597 occurring at the confluence of Deer Creek with the Snake River, Summit County,
598 Colorado. *Environ. Sci. Technol. 26*(7),:1388-1396, doi:10.1021/es00031a017
599 Megonigal, J. P., and S. C. Neubauer. 2009. Biogeochemistry of tidal freshwater wetlands. In
600 *Coastal wetlands: An integrated ecological approach*, ed. G.M.E. Perillo, E. Wolanski,
601 D.R. Cahoon, and M. M. Brinson, 535–562. Amsterdam: Elsevier
602 Mendelssohn, I. A., and J. T. Morris. 2000. Eco-physiological controls on the productivity of
603 Spartina alterniflora Loisel. In M. P. Weinstein & D. A. Kreeger (Eds.), *Concepts and*
604 *Controversies in Tidal Marsh Ecology*, 59-80. Dordrecht: Springer Netherlands.

605 Moore, T. 2009. Dissolved organic carbon production and transport in Canadian peatlands. In A.
606 Baird, L. Belyea, X. Comas, A. Reeve, and L. Slater (Eds.), *Carbon Cycling in Northern*
607 *Peatlands (184):* 229-236, doi: 10.1029/GM184.
608 Moskalski, S. M., and C. K. Sommerfield. 2012. Suspended sediment deposition and trapping
609 efficiency in a Delaware salt marsh. *Geomorphology 139-140*: 195-204, doi:
610 10.1016/j.geomorph.2011.10.018
611 Najjar, R. G., M. Herrmann, R. Alexander, E. W. Boyer, D. J. Burdige, D. Butman, W.-J. Cai, E.
612 A. Canuel, R. F. Chen, M. A. M. Friedrichs, R. A. Feagin, P. C. Griffith, A. L. Hinson, J.
613 R. Holmquist, X. Hu, W. M. Kemp, K. D. Kroeger, A. Mannino, S. L. McCallister, W. R.
614 McGillis, M. R. Mulholland, C. H. Pilskaln, J. Salisbury, S. R. Signorini, P. St-Laurent,
615 H. Tian, M. Tzortziou, P. Vlahos, Z. A. Wang, and R. C. Zimmerman. 2018. Carbon
616 budget of tidal wetlands, estuaries, and shelf waters of eastern North America. *Global*
617 *Biogeochem. Cy.*: 32(3), 389-416, doi:10.1002/2017gb005790
618 Neubauer, S. C. (2008). Contributions of mineral and organic components to tidal freshwater
619 marsh accretion. *Estuar. Coast. Shelf Sci. 78*(1): 78-88, doi: 10.1016/j.ecss.2007.11.011
620 Parfitt, R. L., D. J. Giltrap, and J. S. Whitton. 1995. Contribution of organic matter and clay
621 minerals to the cation exchange capacity of soils. *Commun. Soil Sci. Plan. 26*(9-10):
622 1343-1355, doi:10.1080/00103629509369376
623 Pellegrini, E., F. Boscutti, M. De Nobili, and V. Casolo. 2018. Plant traits shape the effects of
624 tidal flooding on soil and plant communities in saltmarshes. *Plant Ecol. 219*(7): 823-835,
625 doi:10.1007/s11258-018-0837-z
626 Poffenbarger, H. J., B. A. Needelman, and J. P. Megonigal. 2011. Salinity influence on methane
627 emissions from tidal marshes. *Wetlands* 31: 831-842, doi: 10.1007/s13157-011-0197-0

628 Qualls, R. G. 2000. Comparison of the behavior of soluble organic and inorganic nutrients in
629 forest soils. *For. Ecol. Manage. 138*(1-3): 29-50, doi:10.1016/s0378-1127(00)00410-2
630 Riedel, T., D. Zak, H. Biester, and T. Dittmar. 2013. Iron traps terrestrially derived dissolved
631 organic matter at redox interfaces. *Proc. Natl. Acad. Sci. USA, 110*(25): 10101,
632 doi:10.1073/pnas.1221487110
633 Seitzinger, S. P., W. S. Gardner, and A. K. Spratt. 1991. The effect of salinity on ammonium
634 sorption in aquatic sediments: Implications for benthic nutrient recycling. *Estuaries*
635 *14*(2): 167-174, doi:10.2307/1351690
636 Shields, M. R., T. S. Bianchi, Y. Gélinas, M. A. Allison, and R. R. Twilley. 2016. Enhanced
637 terrestrial carbon preservation promoted by reactive iron in deltaic sediments. *Geophys.*
638 *Res. Lett.* 43: 1149-1157, doi:10.1002/2015gl067388
639 Slomp, C. P., S. J. Van Der Gaast, and W. Van Raaphorst. 1996. Phosphorus binding by poorly
640 crystalline iron oxides in North Sea sediments. *Mar. Chem. 52*(1): 55-73,
641 doi:10.1016/0304-4203(95)00078-x
642 Smith, S. J., A. M. Thomson, N. J. Rosenberg, R. C. Izaurralde, R. A. Brown, and T. M. L.
643 Wigley. 2005. Climate change impacts for the conterminous USA: An integrated
644 assessment. *Clim. Change 69*(1): 7-25, doi.org/10.1007/s10584-005-3614-7.
645 Stumm, W., Kummert, R., Sigg, L., 1980. A ligand exchange model for the adsorption of
646 inorganic and organic ligands at hydrous oxide interfaces. *Croat. Chem. Acta* 53: 291–
647 312.
648 Stumm, W., and J. J. Morgan. 2012. *Aquatic Chemistry: Chemical Equilibria and Rates in*
649 *Natural Waters*: Wiley.

650 Tipping, E., C. Rey-Castro, S. E. Bryan, , and J. Hamilton-Taylor. 2002. Al(III) and Fe(III)
651 binding by humic substances in freshwaters, and implications for trace metal speciation.
652 *Geochim. Cosmochim. Acta 66*(18): 3211-3224, doi: 10.1016/S0016-7037(02)00930-4
653 Tobias, C., and S. C. Neubauer. 2019. Chapter 16 - Salt marsh biogeochemistry—An overview.
654 In Perillo, G. M. E., E. Wolanski, D. R. Cahoon, and C. S. Hopkinson (Eds.), Coastal
655 Wetlands (2nd ed.): Elsevier. doi: 10.1016/B978-0-444-63893-9.00016-2
656 Tsutsuki, K., and S. Kuwatsuka. 1984. Molecular size distribution of humic acids as affected by
657 the ionic strength and the degree of humification. *Soil Sci. Plant Nutr. 30*(2): 151-162,
658 doi:10.1080/00380768.1984.10434679
659 Tzortziou, M., P. J. Neale, J. P. Megonigal, C. Pow, and M. Butterworth. 2011. Spatial gradients
660 in dissolved carbon due to tidal marsh outwelling into a Chesapeake Bay estuary. *Mar.*
661 *Ecol. 426*: 41-56, doi:10.3354/meps09017
662 Tzortziou, M., P. J. Neale, C. L. Osburn, J. P. Megonigal, N. Maie, and R. Jaffé. 2008. Tidal
663 marshes as a source of optically and chemically distinctive colored dissolved organic
664 matter in the Chesapeake Bay. *Limnol. Oceanogr. 53*(1): 148-159,
665 doi:10.4319/lo.2008.53.1.0148
666 U.S. DOE. 2017. Research Priorities to Incorporate Terrestrial-Aquatic Interfaces in Earth
667 System Models: Workshop Report, DOE/SC-0187, U.S. Department of Energy Office of
668 Science.
669 Wagai, R., and L. M. Mayer. 2007. Sorptive stabilization of organic matter in soils by hydrous
670 iron oxides. *Geochim. Cosmochim. Acta 71*(1): 25-35, doi:10.1016/j.gca.2006.08.047

671 Wang, Z. A., and W.-J. Cai. 2004. Carbon dioxide degassing and inorganic carbon export from a
672 marsh-dominated estuary (the Duplin River): A marsh CO_2 pump. *Limnol. Oceanogr.*
673 *49*(2): 341-354, doi:10.4319/lo.2004.49.2.0341
674 Watanabe A., K. Moroi, H. Sato, K. Tsutsuki, N. Maie, L. Melling, R. Jaffé. 2012. Contributions
675 of humic substances to the dissolved organic carbon pool in wetlands from different
676 climates. *Chemosphere 88*(10): 1265-1268, 10.1016/j.chemosphere.2012.04.005
677 Williams E. K., B. E. Rosenheim. 2015. What happens to soil organic carbon as coastal marsh
678 ecosystems change in response to increasing salinity? An exploration using ramped
679 pyrolysis: Fate of coastal SOC with salinity. *Geochem. Geophy. Geosy.* 16:2322–2335,
680 doi: 10.1002/2015GC005839
681 Ziegler, S., and R. Benner. 1999. Dissolved organic carbon cycling in a subtropical seagrass-
682 dominated lagoon. *Mar. Ecol. Prog. Ser. 180:* 149-160, doi:10.3354/meps180149
683 Zobeck, T. M. 2004. Rapid soil particle Size analyses using laser diffraction. *Appl. Eng. Agric.*
684 *20*(5): 633-639, doi.org/10.13031/2013.17466

685 .

686 Table 1: Tidal marsh surface characteristics and soil characteristics for 0 - 40 cm depth including standard error.

Characteristic	GCReW	Taskinas Marsh	Jug Bay Marsh	Wachapreague Marsh
Soil Core GPS Coordinates	38°52'25.90"N 76°32'59.60"W	37°24'48.79"N 76°42'57.44"W	38°46'52.32"N 76°42'29.09"W	37°35'56.33"N 75°38'9.38"W
Dominant Vegetation at Soil Core Collection Site	*Schoenoplectus americanus* *Spartina patens* *Distichlis spicata*	*Spartina patens* *Spartina alterniflora* *Distichlis spicata*	*Typha latifolia* *Peltandra virginica* *Nuphar lutea*	*Spartina alterniflora* *Salicornia europaea*
Growing Season Surface Water Salinity (psu)	7.15 ± 0.55	14.8 ± 0	$1.29 \times 10^{-1} \pm 4.50 \times 10^{-3}$	32.0 ± 0
% Soil Organic Matter	74.8 ± 0.2	39.3 ± 1.8	21.8 ± 0.6	5.12 ± 0.54
% Total Organic Carbon	36.2 ± 2.2	12.4 ± 0.3	7.29 ± 0.54	1.77 ± 0.12
Bulk Density (g cm^{-3})	$1.08 \times 10^{-1} \pm 8.11 \times 10^{-3}$	$1.71 \times 10^{-1} \pm 1.25 \times 10^{-2}$	$3.05 \times 10^{-1} \pm 3.42 \times 10^{-2}$	1.99 ± 0.12

687

688 Table 1 (Continued): Tidal marsh surface characteristics and soil characteristics for 0 - 40 cm depth including standard error.

Characteristic	GCReW	Taskinas Marsh	Jug Bay Marsh	Wachapreague Marsh
Specific Surface Area ($m^2\ g^{-1}$)	10.5 ± 0.4	23.8 ± 1.7	40.8 ± 8.1	6.60 ± 1.09
Poorly crystalline Al ($mg\ g^{-1}$)	$5.92 \times 10^{-1} \pm 3.02 \times 10^{-2}$	1.43 ± 0.08	1.22 ± 0.01	$4.64 \times 10^{-1} \pm 1.33 \times 10^{-2}$
Poorly crystalline Fe ($mg\ g^{-1}$)	$1.37 \times 10^{-1} \pm 3.54 \times 10^{-2}$	1.39 ± 0.46	11.2 ± 1.7	1.30 ± 0.28
% Sand	31.6 ± 9.8	46.2 ± 8.4	31.9 ± 6.6	40.6 ± 2.3
% Silt	60.4 ± 7.6	40.8 ± 6.1	57.0 ± 5.3	50.5 ± 2.3
% Clay	8.07 ± 2.4	13.0 ± 2.3	11.1 ± 1.3	8.95 ± 0.13
Mean Grain Size (μm)	39.8 ± 11.9	66.6 ± 30.6	35.2 ± 8.7	49.1 ± 3.2

689

690 Table 2: Mean and standard error of sorption characteristics derived from the Langmuir isotherm
691 by salinity treatment. Q_{max}, C_0, K, and NP refer to the soil maximum sorption capacity, initial
692 exchangeable soil carbon, the DOC binding affinity, and the null point, respectively.

Isotherm Variable	GCReW	Taskinas	Jug Bay	Wachapreague
Q_{max} (mg g^{-1})				
0 psu	2.28 ± 0.39	2.21 ± 0.24	5.85 ± 0.68	4.96 x 10^{-1} ± 4.12 x 10^{-2}
10 psu	4.53 ± 0.45	4.14 ± 0.21	12.2 ± 0.4	1.61 ± 0.25
20 psu	6.57 ± 1.03	7.23 ± 1.81	11.6 ± 0.3	1.73 ± 0.19
35 psu	9.83	10.8	12.5 ± 0.7	2.72 ± 0.53
C_0 (mg g^{-1})				
0 psu	2.11 ± 0.28	1.99 ± 0.18	4.20 ± 0.79	3.71 x 10^{-1} ± 4.79 x 10^{-2}
10 psu	2.10 ± 0.15	2.26 ± 0.25	4.45 ± 0.42	2.88 x 10^{-1} ± 2.801 x 10^{-2}
20 psu	2.06 ± 0.12	1.89 ± 0.14	4.44 ± 0.39	3.74 x 10^{-1} ± 3.59 x 10^{-2}
35 psu	1.98 ± 0.04	1.93 ± 0.06	4.50 ± 0.59	3.50 x 10^{-1} ± 3.06 x 10^{-2}

693

694 Table 2 (Continued)

Isotherm Variable	GCReW	Taskinas	Jug Bay	Wachapreague
K (L g^{-1})				
0 psu	$5.55 \times 10^{-3} \pm 4.44 \times 10^{-3}$	$6.06 \times 10^{-3} \pm 3.24 \times 10^{-3}$	$3.45 \times 10^{-2} \pm 9.60 \times 10^{-3}$	$1.55 \times 10^{-2} \pm 7.80 \times 10^{-3}$
10 psu	$5.17 \times 10^{-3} \pm 1.55 \times 10^{-3}$	$8.44 \times 10^{-3} \pm 2.82 \times 10^{-3}$	$1.01 \times 10^{-2} \pm 2.06 \times 10^{-3}$	$5.04 \times 10^{-3} \pm 1.61 \times 10^{-3}$
20 psu	$3.52 \times 10^{-3} \pm 1.11 \times 10^{-3}$	$2.88 \times 10^{-3} \pm 1.29 \times 10^{-3}$	$1.12 \times 10^{-2} \pm 2.09 \times 10^{-3}$	$6.84 \times 10^{-3} \pm 1.84 \times 10^{-3}$
35 psu	$2.21 \times 10^{-3} \pm 7.18 \times 10^{-5}$	$1.97 \times 10^{-3} \pm 8.91 \times 10^{-5}$	$1.08 \times 10^{-2} \pm 3.08 \times 10^{-3}$	$3.69 \times 10^{-3} \pm 1.22 \times 10^{-3}$
NP (mg L^{-1})				
0 psu	2250	1528	73.9	192
10 psu	167	142	57.1	43.2
20 psu	130	123	55.6	40.3
35 psu	114	110	52.2	40.1
r^2				
0 psu	0.912	0.958	0.991	0.889
10 psu	0.988	0.982	0.995	0.975
20 psu	0.991	0.985	0.996	0.978
35 psu	0.991	0.980	0.992	0.982

695

Table 3: Summary of a linear mixed effects model for sorption isotherm characteristics where [PC-Fe] = soil poorly crystalline iron content, AIC = Akaike information criterion, BIC = Bayesian information criterion, and logLik = log likelihood. Full model summary statistics are presented in the supplementary information.

Log_{10}(Maximum Soil Sorption Capacity), ($Log_{10}(Q_{max})$)

Marginal r^2 (fixed effects only) = 0.636; conditional r^2 (fixed + random effects) = 0.920

Random Effects: Formula: ~1 | Site

	(Intercept)	Residual
StdDev:	3.39×10^{-1}	1.12×10^{-1}

Fixed Effects: $log_{10}(Q)$ ~ Salinity * Fe

	Value	Std Error	DF	t-value	p-value
(Intercept)	1.04×10^{-1}	2.26×10^{-1}	8	4.59×10^{-1}	6.58×10^{-1}
Salinity (psu)	2.36×10^{-2}	4.05×10^{-3}	8	5.82	4.00×10^{-5}
[PC-Fe] (mg g^{-1})	6.68×10^{-2}	3.95×10^{-2}	2	1.69	2.33×10^{-1}
Salinity : [PC-Fe] (psu : mg g^{-1})	-1.36×10^{-3}	5.80×10^{-4}	8	-2.34	4.73×10^{-2}

Table 3 (Continued): Summary of a linear mixed effects model for sorption isotherm characteristics where [PC-Fe] = soil poorly crystalline iron content, AIC = Akaike information criterion, BIC = Bayesian information criterion, and logLik = log likelihood. Full model summary statistics are presented in the supplementary information.

Log_{10}(DOC Binding Affinity),(Log_{10}(K))

Marginal r^2 (fixed effects only) = 0.312; conditional r^2 (fixed + random effects) = 0.803

Random Effects: Formula: ~1 | Site

	(Intercept)	Residual
StdDev:	2.36×10^{-1}	1.49×10^{-1}

Fixed Effects: log_{10}(K) ~ Salinity * Fe

	Value	Std Error	DF	t-value	p-value
(Intercept)	-1.96	1.34×10^{-1}	11	-14.6	0
Salinity (psu)	-1.49×10^{-2}	3.07×10^{-3}	11	-4.86	5.00×10^{-4}

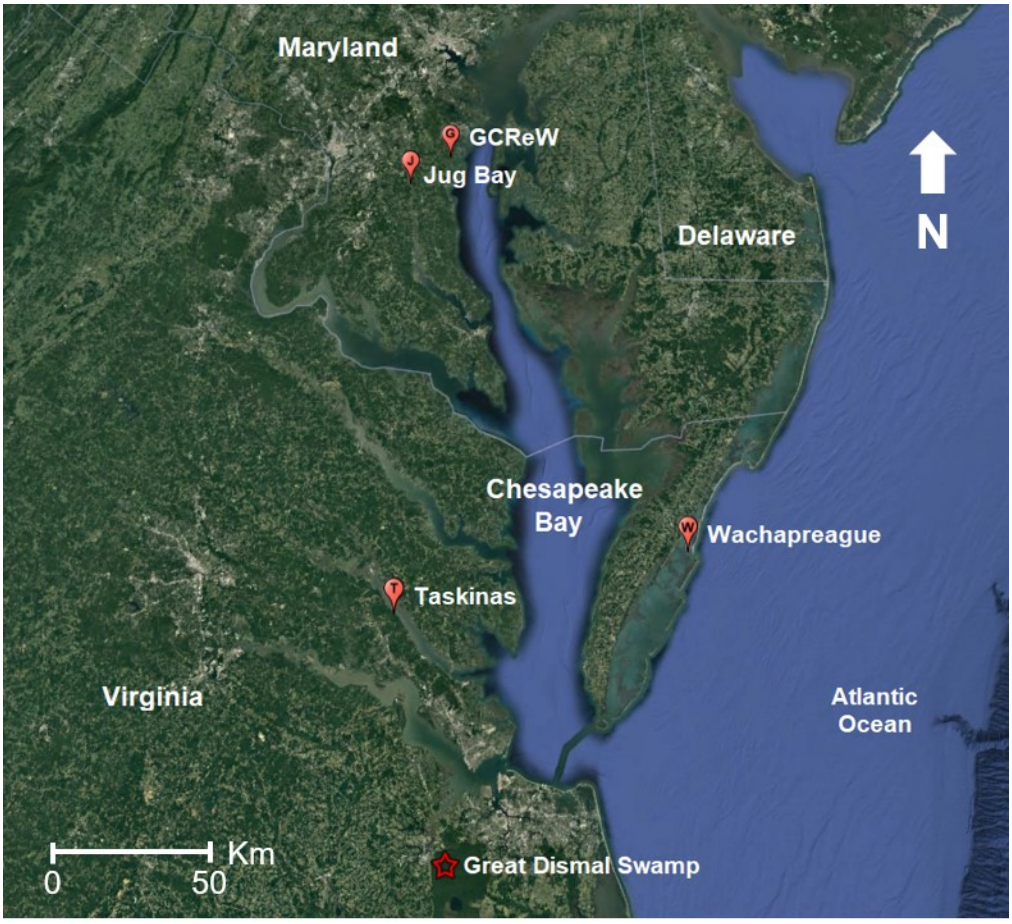

Figure 1: Composite satellite image from Google Earth displaying field site locations. (Google Earth Pro V 7.3.2.5776, March 1, 2019).

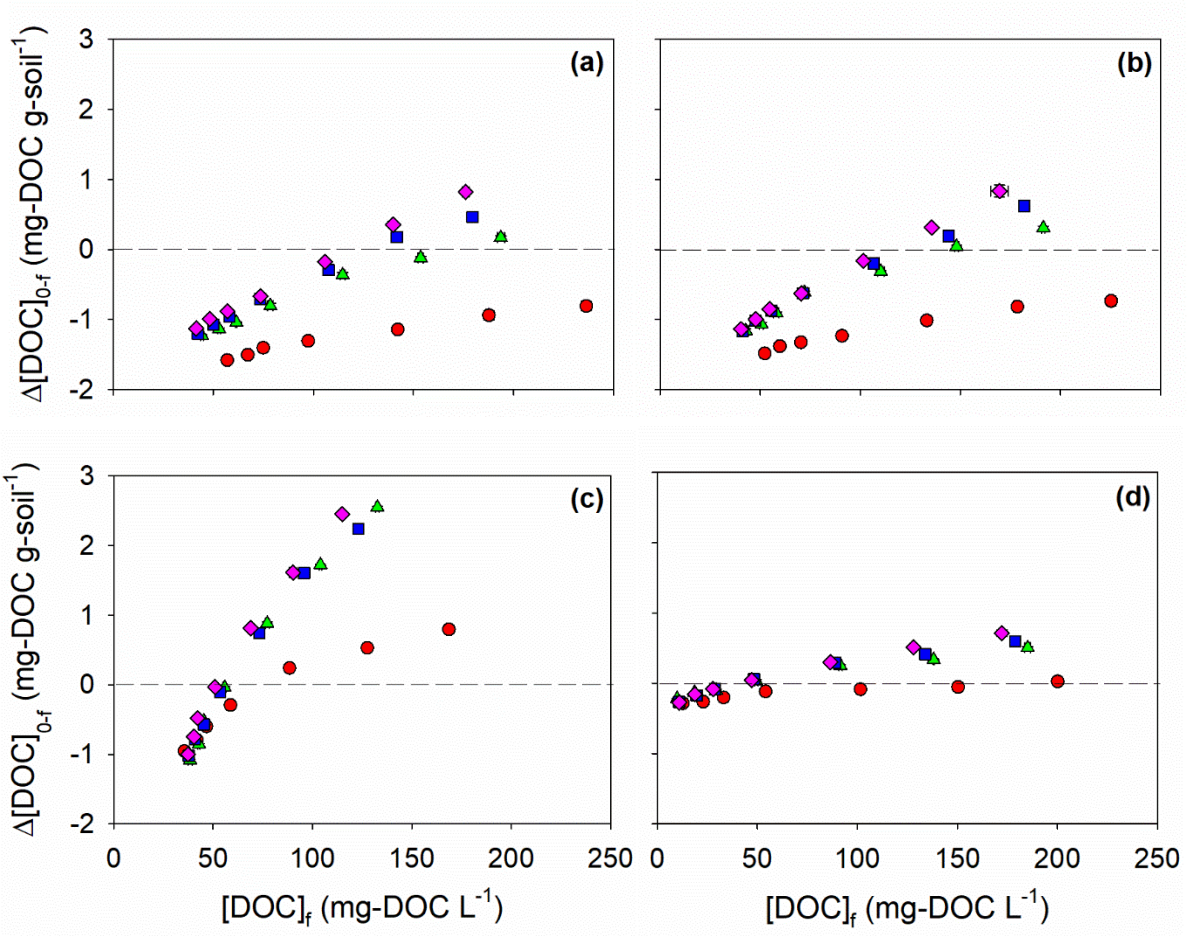

Figure 2: Traditional Langmuir isotherms across the four salinity treatments for (a) GCReW, (b) Taskinas, (c) Jug Bay, and (d) Wachapreague. Red circles, green triangles, blue squares, and purple diamonds reflect 0 psu, 10 psu, 20 psu, and 35 psu salinity treatments, respectively. Bi-directional error bars denote standard error.

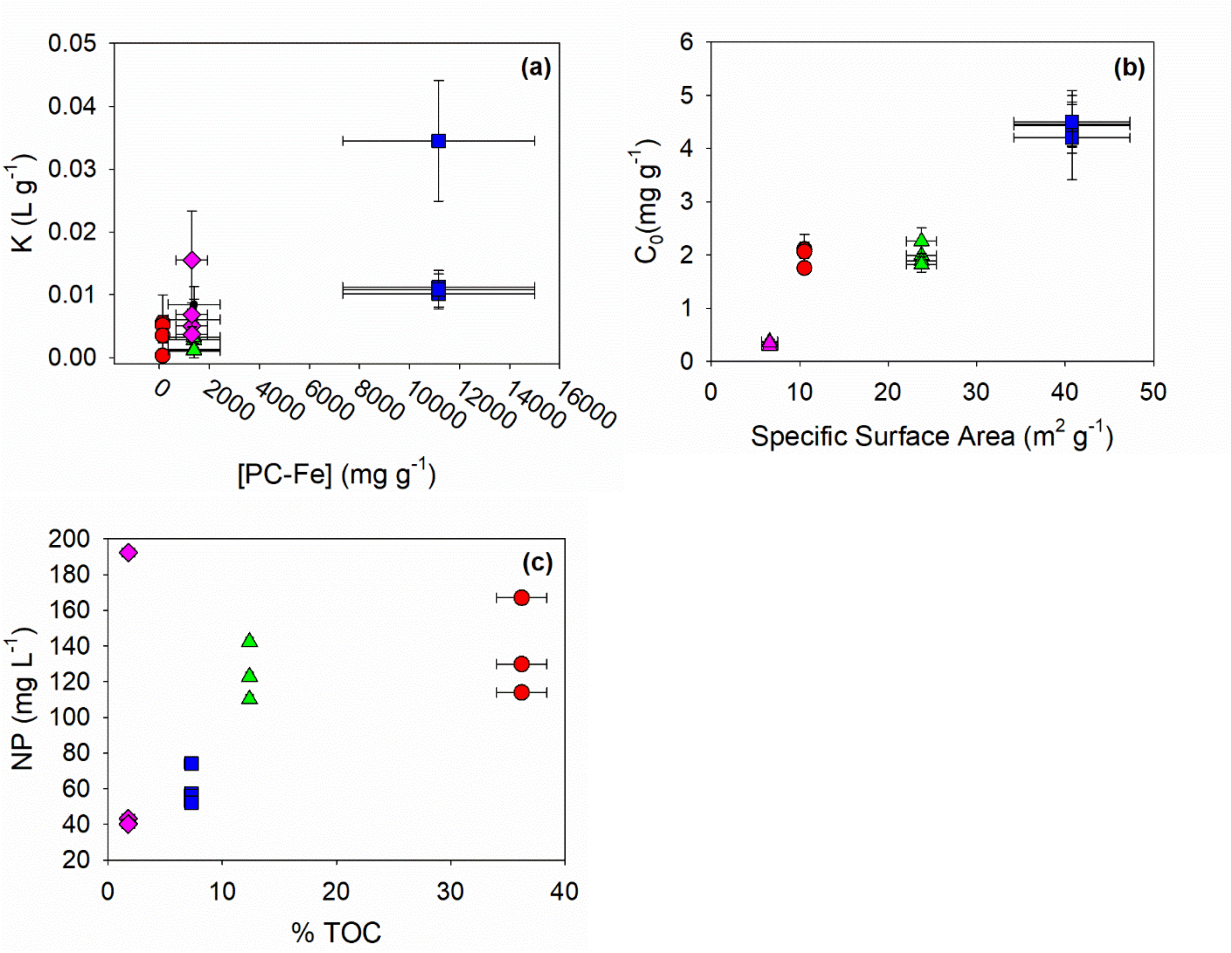

728

729 Figure 3: Scatterplot of (a) poorly crystalline iron ([PC-Fe]) vs DOC binding affinity (Spearman
730 $p = 0.546$, $p = 0.0288$, $n = 16$), (b) soil specific surface area vs natively sorbed DOC (Spearman
731 $p = 0.837$, $p < 0.0001$, $n = 16$), and (c) the percent total organic carbon vs the null point
732 (Spearman $p = -0.610$, $p = 0.0205$, $n = 14$). Red circles, green triangles, blue squares, and pink
733 diamonds reflect GCReW, Taskinas, Jug Bay, and Wachapreague soils, respectively and error
734 bars denote standard error. Please note that values for the GCReW and Taskinas null point at 0
735 psu were omitted from the correlation in graph (c).

736

737

738 **Supplementary Information**

739 Table S1: RStudio code used to run the linear mixed effect models for maximum soil sorption

740 capacity (Qmax) and DOC binding affinity (K).

Isotherm Variable	
Q_{max}	model1.lme <- lme(log10(Q) ~ Salinity * SSA, random = ~ 1 | Site, na.action = na.omit, data = data1)
K	model2.lme <- lme(log10(K) ~ Salinity, random = ~ 1 | Site, na.action = na.omit, data = data1)

741

742

743 Table S2: Summary of the multiple linear regression analysis for soil specific surface area. [PC-
744 Al] = soil poorly crystalline aluminum content and [PC-Fe] = soil poorly crystalline iron content.
745 The analysis was conducted on data from the core depth segments (e.g. 0-5 cm, 5-10 cm, etc.)
746 that make up the bulk soil samples. Standard β refers to parameter estimates where all terms have
747 been standardized to a mean of 0 and a variance of 1 while the variance inflation factor is a
748 measure of the severity of multicollinearity. ($n = 14$; $r^2_{adj} = 0.844$).

Term	Estimate	Std Err	T Ratio	Prob > |t|	Std β	VIF
Intercept	8.56×10^{-1}	3.62	2.40×10^{-1}	0.818	0	
[PC-Al] (mg g^{-1})	13.7	3.56	3.84	2.70×10^{-3}	4.40×10^{-1}	1.09
[PC-Fe] (mg g^{-1})	2.02	3.29×10^{-1}	6.14	$< 1 \times 10^{-4}$	7.03×10^{-1}	1.09

749

750

751 Table S3: Full summary of a linear mixed effects model statistics for maximum soil sorption
752 capacity (Q_{max}) where [PC-Fe] = soil poorly crystalline iron content, AIC = Akaike information
753 criterion, BIC = Bayesian information criterion, and logLik = log likelihood. The marginal r^2
754 (fixed effects only) is 0.636 while the conditional r^2 (fixed + random effects) is 0.920.

Log_{10}(Maximum Soil Sorption Capacity), ($Log_{10}(Q_{max})$)					
AIC	BIC	logLik			
29.7	31.5	-8.84			
Random Effects: Formula: ~1 | Site					
	(Intercept)	Residual			
Std Dev:	3.39×10^{-1}	1.12×10^{-1}			
Fixed Effects: $log_{10}(Q)$ ~ Salinity * PC-Fe					
	Value	Std Error	DF	t-value	p-value
(Intercept)	1.04×10^{-1}	2.26×10^{-1}	8	4.59×10^{-1}	6.58×10^{-1}
Salinity (psu)	2.36×10^{-2}	4.05×10^{-3}	8	5.82	4.00×10^{-5}
[PC-Fe] (mg g^{-1})	6.68×10^{-2}	3.95×10^{-2}	2	1.69	2.33×10^{-1}
Salinity : PC-Fe (psu : mg g^{-1})	-1.36×10^{-3}	5.80×10^{-4}	8	-2.34	4.73×10^{-2}

755

756

Table S3 (continued): Full summary of a linear mixed effects model statistics for sorption isotherm characteristics where [PC-Fe] = soil poorly crystalline iron content, AIC = Akaike information criterion, BIC = Bayesian information criterion, and logLik = log likelihood. The marginal r^2 (fixed effects only) is 0.636 while the conditional r^2 (fixed + random effects) is 0.920.

Correlation:

	(Intercept)	Salinity	PC-Fe
Salinity (psu)	-2.36×10^{-1}		
[PC-Fe] (mg g^{-1})	-6.21×10^{-1}	1.39×10^{-1}	
Salinity : PC-Fe (psu : mg g^{-1})	1.70×10^{-1}	-7.12×10^{-1}	-2.11×10^{-1}

Standardized Within-Group Residuals:

Min	Q1	Med	Q3	Max
-1.10	-4.78×10^{-1}	3.00×10^{-3}	4.30×10^{-1}	1.62

763 Table S4: Full summary of a linear mixed effects model statistics for DOC binding affinity (K)
764 where AIC = Akaike information criterion, BIC = Bayesian information criterion, and logLik =
765 log likelihood. The marginal r^2 (fixed effects only) is 0.312 while the conditional r^2 (fixed +
766 random effects) is 0.803.

Log_{10}(DOC Binding Affinity),(Log_{10}(K))

AIC	BIC	logLik
12.2	14.7	-2.10

Random Effects: Formula: ~1 | Site

	(Intercept)	Residual
Std Dev:	2.36×10^{-1}	1.49×10^{-1}

Fixed Effects: log_{10}(K) ~ Salinity

	Value	Std Error	DF	t-value	p-value
(Intercept)	-1.96	1.34×10^{-1}	11	-14.6	0
Salinity (psu)	-1.49×10^{-2}	3.07×10^{-3}	11	-4.86	5.00×10^{-4}

Standardized Within-Group Residuals

Min	Q1	Med	Q3	Max
-1.39	-5.38×10^{-1}	1.13×10^{-2}	5.68×10^{-1}	1.40

767

768 Figure S1

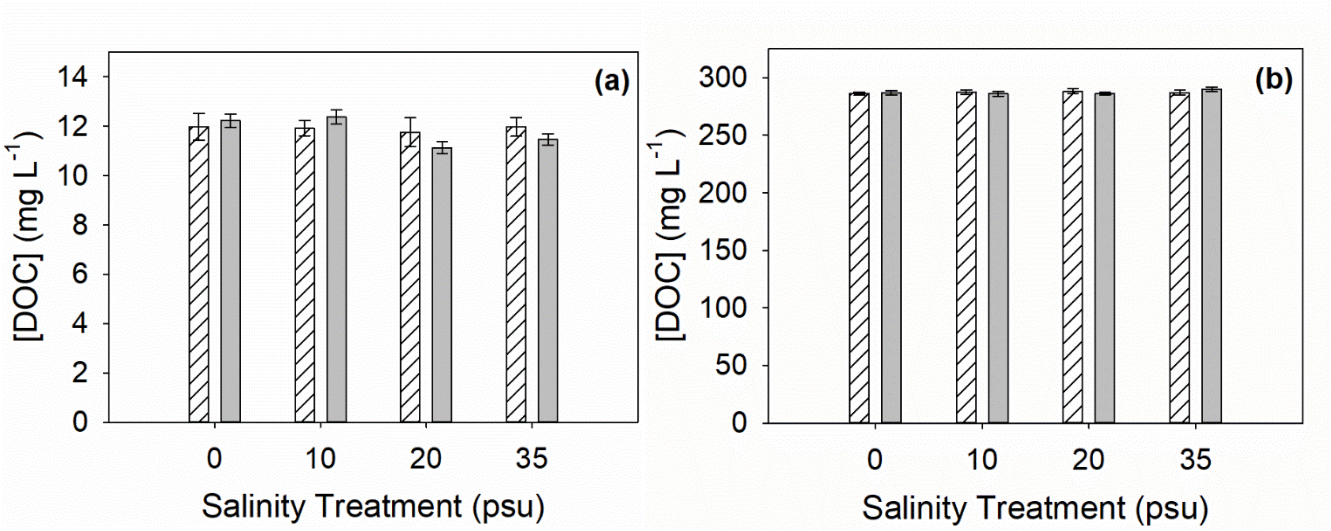

769 Figure S1: Plot of high and low dissolved organic carbon concentration ([DOC]) precipitation
770 test without soil. The patterned bar represents pre-incubation [DOC] and the gray bar represents
771 post-incubation [DOC] across the four salinity treatments for (a) 12.5 mg-DOC L^{-1} stock and (b)
772 285 mg-DOC L^{-1}. Error bars denote standard error (n = 3).